Nanoscale

Accepted Manuscript

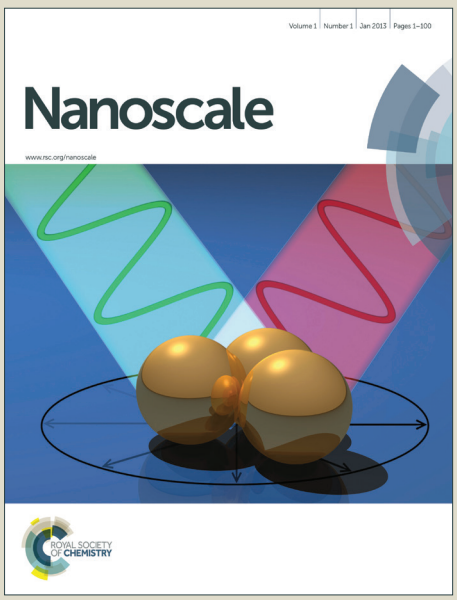

ROYAL SOCIETY OF CHEMISTRY

www.rsc.org/nanoscale

Journal Name

RSCPublishing

ARTICLE

Magnetic Photocatalyst with p-n Junction: Fe_3O_4 Nanoparticle and $FeWO_4$ Nanowire Heterostructure

Cite this: DOI: 10.1039/x0xx00000x

Xuan Cao, Yan Chen, Shihui Jiao, Zhenxing Fang, Man Xu, Xu Liu, Lu Li, Guangsheng Pang* and Shouhua Feng

Received ooth January 2012,
Accepted ooth January 2012

DOI: 10.1039/x0xx00000x

www.rsc.org/

Magnetic n-type semiconductor Fe_3O_4 nanoparticle and p-type semiconductor $FeWO_4$ nanowire heterostructure is successfully synthesized without any surfactants or templates via a facile one-step hydrothermal process at 160 °C. The heterojunction structure and morphology are characterized using X-ray powder diffraction (XRD), transmission electron microscopy (TEM) and high-resolution transmission electron microscopy (HRTEM). Magnetic measurement indicates the coexistence of ferrimagnetic behavior of Fe_3O_4 and weak antiferromagnetic behavior of $FeWO_4$. The degradation of methylene blue (MB) under UV-Visible light irradiation is studied as a model experiment to evaluate the catalytic activity of the $Fe_3O_4/FeWO_4$ heterostructure p-n junctions. The decomposition efficiency is 97.1% after one hour UV-Visible irradiation. This magnetic photocatalyst can be easily recovered from the solution by a permanent magnet and redispersed by removing the magnet.

Introduction

In recent years, there has been growing interest in composite nanostructures integrated with individual building block, such as magnetomicelles, composite semiconducting nanocrystals, semiconductor-metal composite nanostructures, and p-n junctions.[1-4] The p-n type semiconductor composite photocatalyst surface is divided into reduction and oxidation surfaces due to the enhanced excited charge carries separation arising from the juncture between p-type and n-type semiconductors.

Ferberite $FeWO_4$, among various wolframite-type metal tungstates, has attracted considerable attention due to its important technological applications in many areas, including semiconductors, photocatalyst, water splitting, and Li-ion battery, etc.[5-9] $FeWO_4$ is an effective p-type semiconductor photocatalyst with a narrow band gap of 2.0 eV for the degradation of organic pollutants,[7, 8, 10-13] which show visible light response. One limitation of the application for the photocatalysts is that the processes require additional solid-liquid separation steps to separate them from the treated solution to prevent the secondary pollution. Traditional methods for catalysts recovery such as coagulation, flocculation, and sedimentation are quite complex and expensive. Composite photocatalyst with a strong magnetic compound and a photocatalyst could be effectively recovered by applying an external magnetic field, which simplify the recycle procedures.

Magnetic photocatalyst Fe_3O_4/TiO_2 particles, coating of a magnetic iron oxide core with a layer of photoactive titanium dioxide, have been developed.[14,15] However, The composite catalyst exhibits lower photoactivity due to the phase junction of magnetite and titanium dioxide. Due to the large relative energy gap difference between n-type semiconductor TiO_2 (3.2 eV) and n-type semiconductor Fe_3O_4 (0.1 eV), the photogenerated electrons in the exited TiO_2 can be transferred to the lower lying conduction band of Fe_3O_4 and the generated holes can be transferred to the upper lying valence bands of Fe_3O_4. The narrow bandgap of the magnetite enhances the recombination of electron-hole pairs in this case (electron hopping between Fe^{2+} and Fe^{3+} in the lattice), which can explain the low photoactivity of TiO_2/Fe_3O_4 heterostructure compared to the single phase TiO_2. To preserve the photoactivity of TiO_2, an intermediate passive SiO_2 layer is normally used as an electronic barrier to prevent the direct contact between the TiO_2 and Fe_3O_4 phase in the magnetic photocatalyst composite structure $TiO_2/SiO_2/Fe_3O_4$.[16] However, heterojunction structures with appropriate band gaps could promote the charge pairs separation and interfacial charge transfer efficiency, and then effectively enhance the photoactivity. For example, Fe_2O_3/TiO_2 heterogeneous photocatalysts with Fe_2O_3 nanoparticle covered TiO_2 microrods are more active than either pure Fe_2O_3 or TiO_2 under visible light irradiation.[17]

Ferberite $FeWO_4$ may be used as photoactivitied building block in constructing a new magnetic p-n type photocatalyst

with n-type semiconductor Fe_3O_4. Methods available for nanoparticle combination include the sol-gel technique, the aerosol combustion technique, and the chemical vapour deposition, etc. All the methods need the multi-stepped procedures using monodispered nanoparticles as precursor. Furthermore, many efforts have been made for the preparation of $FeWO_4$ with various morphologies such as hierarchical plate, nanorods, nanowires and spindle-like nanoparticles.[18-20]

In this paper, a facile hydrothermal method is developed to synthetize magnetic heterostructure photocatalyst with n-type Fe_3O_4 nanoparticles and p-type $FeWO_4$ nanowires in one step. The hierarchical structure and magnetic property of the p-n type semiconductor composite photocatalysts have been further studied. The photocatalytic property of the composite stucture is examined using methylene blue (MB) and the magnetic photocatalyst can be easily recovered by applying a magnetic field.

Experimental

Materials

Iron(II) sulfate heptahydrate ($FeSO_4 \cdot 7H_2O$, AR), Tungstic acid (H_2WO_4, AR) and Lithium hydroxide monohydrate ($LiOH \cdot H_2O$, AR) are used as the starting materials. Methylene blue trihydrate is used as dyes. All are purchased from Sinopharm Chemical Reagent Co., Ltd (Shanghai, China) and used without further purification. Deionized water is used throughout.

Preparation of the $Fe_3O_4/FeWO_4$ Heterostructure

The samples are prepared by a hydrothermal process without any templates. $LiOH \cdot H_2O$, H_2WO_4, and $FeSO_4 \cdot 7H_2O$ which in a molar ratio for Li : Fe : W = 3 : 1 : 1 are dissolved in 30 mL distilled water under magnetic stirring. The pH of the solution is 7.5. The solution is transferred into a 45 mL Teflon-lined stainless steel autoclave and maintained at 160 °C for 24 h. After cooling down to room temperature, precipitates are washed with deionized water using a small permanent magnet. The deposited precipitates are subjected to vacuum drying to obtain the final products.

Measurement of Photocatalytic Activity

Photocatalytic activity is evaluated by the degradation of methylene blue under UV-Visible light irradiation using a 500 W Xe lamp with an intensity f ≈120 mW/cm^2 and summer sunlight with an intensity f ≈ 54 mW/cm^2 in a range of 300-1,000 nm, respectively. The corresponding light intensity was tested using a light intensity meter (TENMARS TM-207). Experiments are carried out at ambient temperature as follows: the catalyst (20 mg) is suspended in MB solution (50 mL, 20 mg/L). Before illumination, the aqueous suspension is mechanically stirred for 1 h in the dark to ensure the establishment of an adsorption-desorption equilibrium between photocatalyst and MB. Then, the suspension is exposed to UV-Visible irradiation or sunlight under continuous stirring. During irradiation, the reactant solution is withdrawn at regular intervals. The catalysts are separated with the help of a NdFeB magnet and the residual dye concentration are monitored by measuring the absorbance of the solution at 665 nm[21,22] with a UV-2450 UV-Visible spectrophotometer. Another MB solution without the samples follows the same procedures as the blank tests. All the experiments are conducted three times and the average values are reported.

Characterization

The XRD patterns are obtained by a PANalytical B.V. Empyrean X-Ray Powder Diffractometer with Cu Kα radiation over a range of 10-90° (2θ) with 0.02°/step. Transmission electron microscopy (TEM) images are obtained using a Tecnai G2 FEI Company electron microscope with conventional sample preparation and imaging techniques. XPS spectra are performed on a Thermo ESCALAB 250 with Al Kα radiation at θ = 90° for the X-ray sources, the binding energies are calibrated using the C1s peak at 284.8 eV. UV-Visible solid absorbances of the samples were obtained using a UV-Visible solid spectrometer (PerkinElmer Lambda950) by using $BaSO_4$ as a reference. The magnetic properties are investigated with a Quantum Design SQUID-VSM. Both zero field cooling (ZFC) and field cooling (FC) processes from 2 to 300 K are measured under an applied field of 100 Oe. Magnetic hysteresis loops are measured at 300 K under magnetic field up to 3 T.

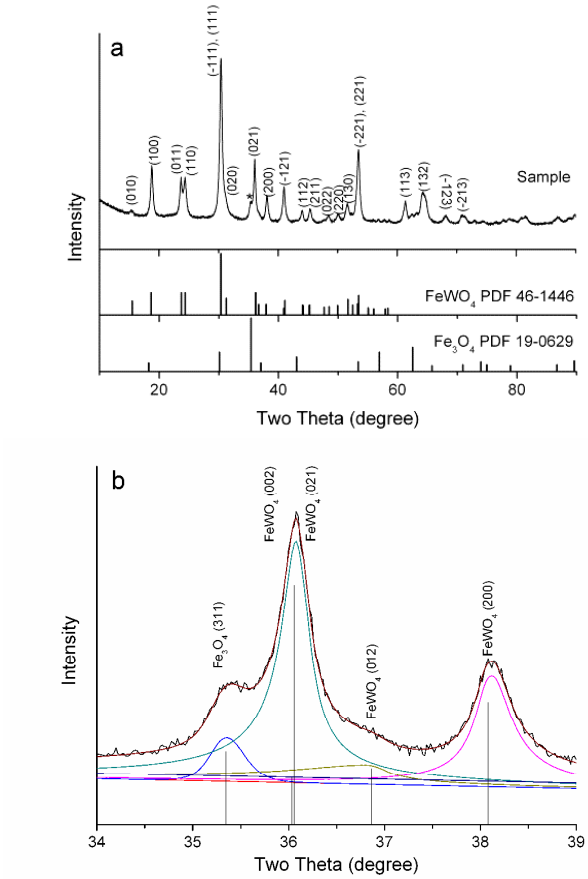

Fig. 1 (a) Indexed powder XRD pattern of the $Fe_3O_4/FeWO_4$ products and ICDD files of Fe_3O_4 and $FeWO_4$. (b) Profile refined by Pearson-VII distribution.

Results and discussion

Fig. 1 shows X-ray diffraction patterns (XRD) of the obtained $Fe_3O_4/FeWO_4$ products. The reflection peaks without asterisk mark are well indexed as $FeWO_4$ monoclinic phase with space group P2/C reported in the ICDD file (PDF file No.: 46–1446),[23] which prove that the main phase of the composite is ferberite $FeWO_4$ as shown in Fig. 1a. The peak with asterisk mark is attributed to the reflection of Fe_3O_4 phase. The diffraction profile of the sample containing strongest (311) reflection peak of Fe_3O_4 is refined by Pearson-VII distribution, as shown in Fig. 1b. The diffraction peak of the Fe_3O_4 phase is quite weak compared with the crystalline diffraction peaks of $FeWO_4$.

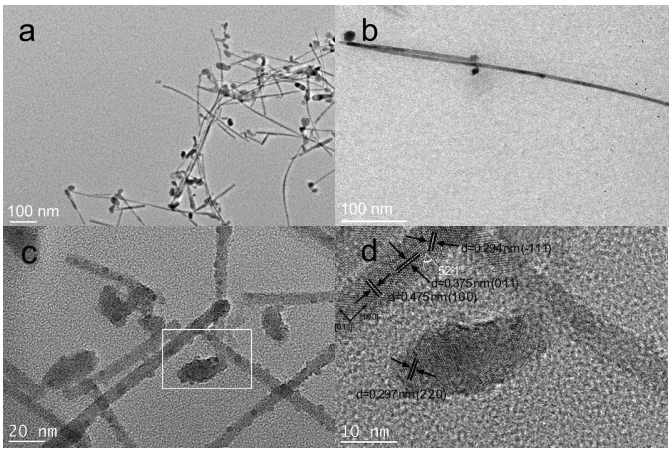

Fig. 2 TEM image of $Fe_3O_4/FeWO_4$ (a) Low-magnification TEM image. (b, c) High-magnification TEM image. (d) High resolution TEM image of the nanowire and nanoparticle.

A typical transmission electron microscopy (TEM) is used to further study the morphology and structure of the composite. Fig. 2a displays a representative low-magnification TEM image of as-synthesized $Fe_3O_4/FeWO_4$ composites, which show the architecture is built by nanowires and nanoparticles. The nanowires show the similar size and shape, but the nanoparticles are highly variable in sizes and in morphologies. The high-magnification TEM images (Fig. 2b and 2c) reveal the nanowires with an average diameter about 10 nm, and lengths from 200 to 500 nm. It is of interest that the nanoparticles are found attaching randomly on the surface of the nanowires to form the heterojunction structure. The HRTEM image (Fig. 2d) shows clear lattice fringes of a separated nanowire and an individual nanoparticle, which is taken from the center region in Fig. 2c. The observed lattice spacings of 4.75 Å, 3.75 Å, and 2.94 Å correspond to the interplanar spacings of the (100), (011), and (-111) planes of the monoclinic $FeWO_4$ structure, respectively. The observed angle between (100) plane and (-111) plane is 52.1 degrees, which is quite close to the theoretical value of 51.7 degrees. It clearly indicated the $FeWO_4$ nanowires grew along the [100] direction.[9] The periodic fringe spacing confirmed that the $FeWO_4$ nanowire is a single crystalline structure. The lattice spacing of nanoparticle is 2.97 Å which corresponds to the (220) interplanar spacing of Fe_3O_4.

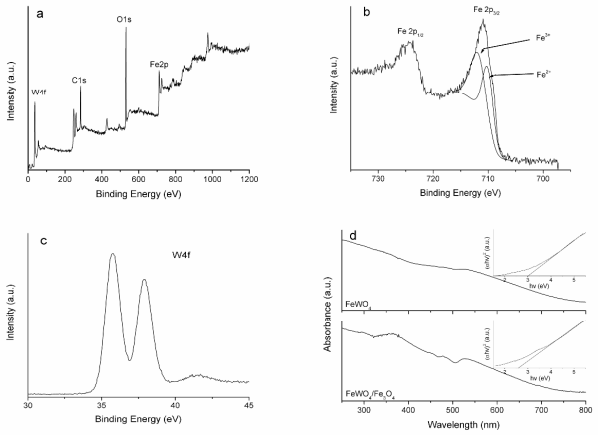

Fig. 3 (a) XPS spectra of magnetic composite $Fe_3O_4/FeWO_4$, (b) Fe 2p ,(c) W 4f, (d) UV-Visible spectra of $FeWO_4$ and $FeWO_4/Fe_3O_4$.

Fig. 3a shows the full spectrum of XPS of magnetic composite $Fe_3O_4/FeWO_4$. The main peaks at 35.5, 283.6, 530.7, and 710.9 eV can be attribute to the binding energies of W_{4f}, C_{1s}, O_{1s}, and Fe_{2p}, respectively.[6] In Fig. 3b, the peak value at 710.9 and 723.7 eV are assigned to the binding energies of Fe $2p_{3/2}$ and Fe $2p_{1/2}$, respectively. No satellite at 719 eV can be observed. This is consistent with the mixed valence Fe ions in Fe_3O_4.[24-26] The Fe $2p_{3/2}$ peak is deconvoluted into the Fe^{2+} and Fe^{3+} peaks.[24] In Fig. 3c, two peaks located at 35.5 and 37.8 eV are assigned to W 4f with binding energies corresponding to those of tungsten in the formal valence +6.[27] UV-Visible spectra of the as-prepared $Fe_3O_4/FeWO_4$ and pure $FeWO_4$ nanowires were shown in Fig. 3d. The band gaps of the $Fe_3O_4/FeWO_4$ and pure $FeWO_4$ were also calculated (ESI). The band gap of $FeWO_4$ was estimated to be 3.0 eV, which was significantly wider than the general band gap of 2.0 eV for bulk $FeWO_4$ due to quantum size effect of the nanostructure.[8] The morphology and grain size of $FeWO_4$ nanowire played a important role in increasing the band gap. For the $Fe_3O_4/FeWO_4$ heterojunction, the band gap was estimated to be 2.5 eV, which was narrower than the pure $FeWO_4$ nanowires. It indicated that the Fe_3O_4 significantly influenced the band gap structure of $Fe_3O_4/FeWO_4$.

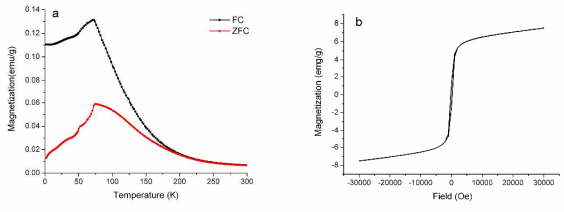

Fig. 4 (a) Temperature dependence of magnetization curves measured with applied field of 100 Oe under FC and ZFC conditions. (b) Magnetization hysteresis (M-H) loops measured at 300 K. Inset shows an enlarged area of the center of the M-H loops.

The temperature dependent magnetization of the $Fe_3O_4/FeWO_4$ composite nanostructures is measured under ZFC and FC procedures are shown in Fig. 4a. The ZFC and FC curves overlap at high temperature above T_{rev} = 200 K, exhibiting the superparamagnetic behavior. ZFC and FC curves are irreversible below T_{rev}, and some Fe_3O_4 nanoparticles are blocked in this temperature range. It is also supported by the magnetic hysteresis of the magnetic composite $Fe_3O_4/FeWO_4$ measured at room temperature as shown in Fig. 4b. The quick saturated hysteresis reveals a superparamagnetism-like loop with saturation magnetization (*M*s), remnant magnetization (*M*r), and coercivity (*H*c) of 9 emu/g, 1.2 emu/g, and 217 Oe, respectively. For the field cooling (FC) magnetization curve, the magnetization initially shows a rapidly increase with decreasing temperature from 300 K to 76 K, and then the magnetization is decreased slowly. The magnetization in the ZFC process increased to the maximum at 76 K with increasing temperature and then decreased, which has nearly the same trend as that of FC curve. Therefore, it may be speculated that the magnetic behavior of the $Fe_3O_4/FeWO_4$ heterostructure at low temperature below T_{peak} derives from the antiferromagnetic property of $FeWO_4$.[13]

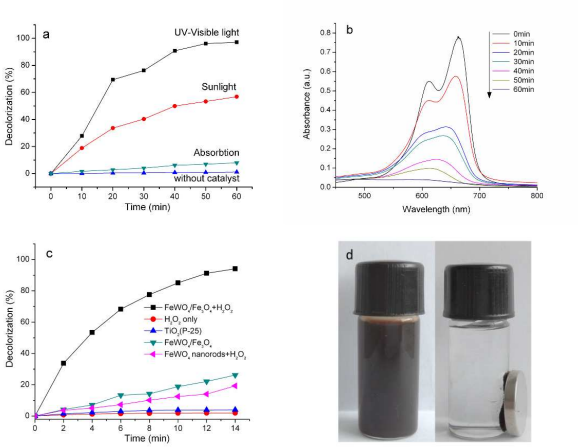

Fig. 5 (a) Degrading efficiency at different time with $Fe_3O_4/FeWO_4$ catalyst under UV-Visible light and summer sunlight, respectively. (b) Absorption spectrum of the MB solution in the presence of $Fe_3O_4/FeWO_4$ composite photocatalyst under UV-Visible light. (c) Degrading efficiency at different time with various catalysts under summer sunlight. (d) Photographs of $Fe_3O_4/FeWO_4$ composite photocatalyst suspension before and after magnetic separation.

The photocatalytic activity of magnetic $Fe_3O_4/FeWO_4$ heterostructure is evaluated for MB degradation under UV-Visible light and summer sunlight, as shown in Fig. 5. Degrading efficiency under UV-Visible light and sunlight is shown in Fig. 5a. It tells that with $Fe_3O_4/FeWO_4$ photocatalyst, the degrading efficiency increases rapidly during the first 20 min. Then slowly get to 97.1% at 60 min under UV-Visible light. The degrading efficiency under sunlight is lower than that under UV-Visible light, but still close to 60% at 60 min. The blank test displays that the degradation of MB can be ignored after 60 min of irradiation without photocatalyst, indicating that $Fe_3O_4/FeWO_4$ magnetic photocatalyst is the key factor in the photodegradation of MB.[12] Fig. 5b shows that the intensity of the 665 nm absorption band decreased rapidly following the reaction process with increasing irradiation time, indicating the degradation of the dye molecules. Photocatalytic degradation of MB with various photocatalysts is evaluated under sunlight. $Fe_3O_4/FeWO_4$ composite photocatalyst is more active than $FeWO_4$ nanorods[9] and TiO_2 (P25), as shown in Fig. 5c. Addition of H_2O_2 (15mmol/L) into the MB solution strongly promoted the degradation due to the generated $^{\bullet}OH$ from H_2O_2 during the photocatalysis procedure. The $^{\bullet}OH$ can oxidize almost all electron rich organic molecules, and convert them to CO_2 and H_2O. After the photo-degradation procedures, the dissolved Fe ions in the solution were evaluated by ICP. The concentration of Fe ions is 0.001 mmol/L, which proves the high stability of the $Fe_3O_4/FeWO_4$ composite photocatalyst during the MB degradation process.[28] The synthesized $Fe_3O_4/FeWO_4$ magnetic photocatalyst can be easily recovered from the solution by a permanent magnet as shown in Fig. 5d.

In conventional photocatalyts, the photoinduced electrons and holes migrate randomly and the recombination of the charge carries reduce quantum yield in the catalytic process. The p-n type semiconductor composite nanostructures could exhibit the advantages of the pristine building blocks and the p-n junction. When a p-n junction is constructed in a photocatalytic system, the excited charge carries will immediately separate under internal electrostatic field in the p-n junction region and then move the electron and hole in opposite directions to retard the recombination and increase quantum yield. For this situation, the Fe_3O_4 has a higher work function and Fermi level than $FeWO_4$. The photoexcited electrons migrate from $FeWO_4$ to Fe_3O_4 through the junction, which provide the Fe_3O_4 an excess electrons (reduction region) and leave $FeWO_4$ localized excess oles (oxidation region), as shown in Fig. 6. In this way, the $Fe_3O_4/FeWO_4$ p-n junction shows enhanced photoactivity for organic pollution degradation under sunlight.

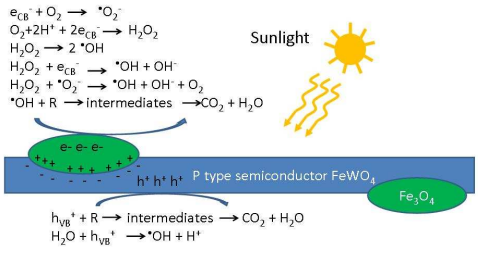

Fig. 6 Principle of photocatatic degradation of organic pollutants on the surface of $Fe_3O_4/FeWO_4$ composite photocatalyst.

Conclusions

In summary, we have developed a template-free hydrothermal method to synthesize $Fe_3O_4/FeWO_4$ magnetic photocatalyst at low temperature 160 °C. The XRD patterns show that $FeWO_4$

is attributed to monoclinic phase with space group P2/C. The TEM results indicate that the crystalline $FeWO_4$ nanowires grow along the *a*-axis. The average width of the nanowires is about 10 nm and the length of the nanowires is from 200 to 500 nm. The n-type Fe_3O_4 nanoparticles grow on the surface of the p-type $FeWO_4$ nanowires to form the p-n heterojunction. By UV–Visible analyses, the band gap of the $Fe_3O_4/FeWO_4$ magnetic photocatalyst is calculated to be 2.50 eV, indicating that the $Fe_3O_4/FeWO_4$ heterojunction has a suitable band gap for photocatalytic degradation of organic pollutants under visible light irradiation. The sample exhibits superparamagnetic-like property sourced from Fe_3O_4 nanoparticles. Meanwhile, the samples display high photocatalytic activity under UV-Visible light and sunlight. When exposed to UV-Visible light for one hour, a removal efficiency of 97.1% for MB is observed. After the degradation process, $Fe_3O_4/FeWO_4$ photocatalysts can be easily separated from the suspension by applying an external magnetic field.

Acknowledgements

This work is supported by the National Natural Science Foundation of China (no. 21071058, 21371066, and 21301067).

Notes and references

*State Key Laboratory of Inorganic Synthesis and Preparative Chemistry, College of Chemistry, Jilin University, Changchun 130012, P. R. China
Address correspondence to panggs@jlu.edu.cn

†Electronic Supplementary Information (ESI) available: Equation used to calculate the energy band gap, XRD of the products with various pH values, SEM image of $Fe_3O_4/FeWO_4$, TEM image of $FeWO_4$ nanowires. See DOI: 10.1039/b000000x/

1 B. S. Kim, J. M. Qiu, J. P. Wang and T. S. Taton, *Nano Lett.*, 2005, **10,** 1987-1991.
2 R. Peter, M. Protiere and Liang Li, *Small*, 2009**, 5,** 154-168.
3 C. L. Yu, G. Li, S. Kumar, K. Yang and R. C. Jin, *Adv. Mater.*, 2014, **26**, 892–898.
4 T. Wang, M. S. Si, D. Z. Yang, Z. Shi, F. C. Wang, Z. L. Yang, S. M. Zhou and D. S. Xue, *Nanoscale*, 2014, **6**, 3978-3983.
5 W. B. Hu, Y. Zhao, Z. Liu, C.W. Dunnill, D.H. Gregory and Y. Zhu, *Chem. Mater.*, 2008, **20,** 5657-5665.
6 Y. X. Zhou, H. B. Yao, Q. Zhang,J. Y. Gong, S. J. Liu and S. H. Yu, *Inorg. Chem*. 2009, **48,** 1082-1090.
7 S. Rajagopal, D. Nataraj, O. Y. Khyzhun, Y. Djaoued, J. Robichaud and D. Mangalaraj, *J. Alloy. Compd.*, 2010, **493**, 340-345.
8 J. Zhang, Y. Wang, S. K. Li, X. F. Wang, F. Z. Huang,A. J. Xie and Y. H. Shen, *CrystEngComm*, 2011, **13,** 5744-5750.
9 H. W. Shim, I. S. Cho, K. S. Hong, W. I. Cho and D. W. Kim, *Nanotechnology*, 2010, **21**, 465-602.
10 H. X. Li, X. Y. Zhang, Y. N. Huo and J. Zhu, *Environ. Sci. Technol.*, 2007, **41**, 4410-4414.
11 D. F. Zhang and F. B. Zeng, *J. Mater. Sci.,* 2012, **47**, 2155-2161.
12 J. Guo, X. Zhou, Y. Lu, X. Zhang, S. Kuang and W. Hou, *J. Solid State Chem.,* 2012, **196**, 550-556.
13 J. Zhang, Y. Zhang, J. Y. Yan, S. K. Li, H. S. Wang, F. Z. Huang, A and J. Xie, *J. Nanopart. Res.,* 2012, **14,** 1-10.
14 X. Q. Zhang, Y. H. Zhu, X. L. Yang, Y. Zhou, Y. F. Yao and C. Z. Li, *Nanoscale*, 2014, **6**, 5971-5979.
15 Y. Yuan, S. Chen, T. Paunesku, S. C. Gleber, W. C. Liu, C. B. Doty, R. Mark. J. J. Deng, Q. L. Jin, B. Lai, K. Brister, C. Flachenecker, C. Jacobsen, S. Vogt and G. E. Woloschak, *ACS nano*, 2013, **7**, 10502-10517.
16 D. Beydoun, R. Amal, G. Low and S. McEvoy, *J. Mol. Catal. A-Chem.,* 2002, **180**, 193-200.
17 L. L. Peng, T. F. Xie, Y. C. Lu, H. M. Fan and D. J. Wang, *Phys. Chem. Chem. Phys.,* 2010, **12**, 8033-8041.
18 E. Schmidbauer, U. Schanz and F. J. Yu, *J. Phys.-Condens. Mat.,* 1991, **3**, 5341-5352.
19 S. H. Yu, B. Liu, M. S. Mo, J. H. Huang, X. M. Liu and Y. T. Qian, *Adv. Funct. Mater.,* 2003, **13**, 639-647.
20 L. L. Xing, P. Deng, B. He, Y. X. Nie, X. L. Wu, S. Yuan, C. X. Cui and X. Y. Xue, *Electrochim. Acta*, 2014, **118**, 45-50.
21 T. J. Yao, T. Y. Cui, H. Wang, L. X. Xu, F. Cui and J. Wu, *Nanoscale*, 2014, **6**, 7666-7674.
22 C. Quinones, J. Ayala and W. Vallejo, *Appl. Surf. Sci.,* 2010, **257**, 367-371.
23 S. Rajagopal, V. L. Bekenev, D. Nataraj, D. Mangalaraj and O. Y. Khyzhun, *J. Alloy. Compd.,* 2010, **496**, 61-68.
24 T. Yamashita and P. Hayes, *Appl. Surf. Sci.,* 2008, **254,** 2441-2449.
25 D. D. Hawn and B. M. DeKoven, *Sur. Interface Anal.,* 1987, **10** 63-74.
26 M. Muhler, R. Schlögl and G. Ertl, *J. Catal.,* 1992, **138**, 413-444.
27 O. Y. Khyzhun, *J. Alloy.Compd.,* 2000, **305,** 1-6.
28 Z. He, C. Gao, M. Qian, Y. Shi, J. Chen and S. Song, *Ind. Eng. Chem. Res.* **2014**, 53, 3435-3447.